Journal of Wind Engineering & Industrial Aerodynamics 245 (2024) 105634



Contents lists available at ScienceDirect

Journal of Wind Engineering & Industrial Aerodynamics

journal homepage: www.elsevier.com/locate/jweia





Thunderstorm impact on the built environment: A full-scale measurement and post-event damage survey case study

Ileana Calotescu [a], Xiao Li [b,*], Mekdes T. Mengistu [b], Maria Pia Repetto [b]

[a] Department of Steel Structures, Management and Engineering Graphics (DCMMGI), Technical University of Civil Engineering Bucharest, Bd. Lacul Tei, 122-124, 020396 Bucharest, Romania
[b] Department of Civil, Chemical and Environmental Engineering (DICCA), Polytechnic School, University of Genoa, Via Montallegro, 1, 16145 Genoa, Italy

ARTICLE INFO

Keywords:
Damage survey
Wind-induced damage
Hail-induced damage
Thunderstorms
Wind field measurement

ABSTRACT

This paper investigates the impact of an intense thunderstorm on the urban area of Sânnicolau Mare, Romania, based on the meteorological data collected by full-scale field measurement and the damage data of low-rise buildings obtained by post-event survey. The meteorological data throughout the entire thunderstorm process were collected from two sources, namely, a wind and structural monitoring system of a 50 m-tall lattice tower and a state-operated meteorological station, both located at the outskirts of the city. The damage data were collected by post-event in-situ survey with crowdsourcing techniques, providing information of both wind- and hail-induced damage to over 200 low-rise buildings. Based on the meteorological and damage data, the damage mechanisms were revealed by conducting forensic engineering analysis for two representative buildings which respectively sustained severe wind- and hail-induced damage. Moreover, the widely used estimation scales for wind intensities, such as the Fujita scale, were validated by anemometric records and damage observations. Finally, the feasibility of utilizing the hail-induced damage to building facades as a new indicator for the estimation of wind speed and direction was discussed. This study aims to further understand the impact of thunderstorms on low-rise buildings, so as to deliver essential information for their storm-resistant designs.

1. Introduction

Windstorms constitute one of the most dangerous and costly natural hazards in Europe and worldwide, causing economic losses and risks for people. The European Environment Agency (EEA; https://www.eea.europa.eu) reported that weather- and climate-related extremes in the EEA Member States caused 80% of total economic losses due to natural hazards between 1980 and 2020. The total amount of fatalities damaged by windstorms over the period 1980–2020 summed up to an average of 80/year and the total reported economic losses reached an average of 3.7 billion Euros/year.

Extreme wind events range from mesoscale long-lasting synoptic phenomena, like extratropical cyclones, to microscale short events, in particular tornadoes and thunderstorm outflows which are often responsible for the strongest winds and worst impacts. Windstorms related to larger phenomena are easier to measure and forecast; their effects on structures have been analyzed and modeled since the pioneering work of Davenport (1961) and are well integrated into standards and codes. Thunderstorms, on the other hand, are small-spaced and rapidly evolving phenomena, whose measurement and forecast are challenging. Due to the scarce availability of data, models of the outflows and of their effects on the built environment are still matters of research and are not covered by standards and codes. Thunderstorm-induced damage to the built environment is of major concern, given that thunderstorms were responsible for approximately 20% of building damage in the 20th century (Blong, 2004). Cases of thunderstorm-induced damage to buildings are widely available in literature, especially those related to light-frame low-rise buildings (Chmielewski et al., 2013; Cox et al., 2019; Tamura, 2009). Meanwhile, recent studies suggested that, possibly as a consequence of anthropogenic global warming, both the frequency and the intensity of thunderstorms are increasing (Kunz et al., 2009; Rädler et al., 2019; Stott et al., 2016). Hence, in order to improve global resilience against meteorological hazards, there is an urgent need to further investigate the impact of thunderstorms on the built environment.

The modern study of thunderstorms started with key atmospheric sciences projects (Byers and Braham, 1949; Fujita, 1985) which demonstrated that they typically originate from local surface

* Corresponding author.
E-mail address: xiao.li@edu.unige.it (X. Li).

https://doi.org/10.1016/j.jweia.2023.105634
Received 24 March 2023; Received in revised form 26 September 2023; Accepted 20 December 2023
Available online 16 January 2024
0167-6105/© 2024 The Authors. Published by Elsevier Ltd. This is an open access article under the CC BY license (http://creativecommons.org/licenses/by/4.0/).

convection. Thunderstorms evolve in about 30 min and generate a downdraft of cold air that, after impinging at the ground, produces intense radial outflows characterized by non-stationary velocity fields with a "nose-shaped" profile with the maximum at about 40–60 m height (Hjelmfelt, 1988). In parallel, striking research arose in the wind engineering sector, mainly oriented to monitoring, modeling, and simulating thunderstorm outflows, wind actions, and structural response (Letchford et al., 2002; Solari, 2014; Solari et al., 2020; Mengistu et al., 2023). Among many different approaches, experimental campaigns are key factors to improve the physical knowledge of thunderstorms and their effect on structures. Wind tunnel testing on scaled models is a common practice in wind engineering, both for flow modeling and structural aerodynamic analyses. However, reproducing the non-stationary characteristics of thunderstorm downbursts in conventional boundary layer wind tunnels is still challenging. Recently, blade systems and smart devices were proposed to simulate the transient nose-shaped wind profiles effect (Aboutabikh et al., 2019; Ghazal et al., 2022; Le and Caracoglia, 2020). In parallel, novel facilities with particular experimental setups were realized worldwide, such as the "WindEEE Dome" (Canepa et al., 2022; Jubayer et al., 2016), the "Three Little Pigs" (Kopp et al., 2012) at Western University, the "Wall of Wind" (Leatherman et al., 2007) at Florida International University, and the multiple-fan wind tunnel (Brusco et al., 2022; Mason and Lo, 2019) of the Tamkang University, which provided useful references for the studies on downburst outflows and damage induced thunderstorms, but still limited to few configurations.

Efforts were also devoted to full-scale field measurement projects, to assess the thunderstorm outflows (Canepa et al., 2020) and their characteristics relevant to structural response (Lombardo et al., 2014, 2018; Solari et al., 2020; Zhang et al., 2018). However, due to their small spatial-temporal scales, it is very rare to capture thunderstorm events in free field experimental campaigns; thus, it is difficult to detect the effect of many factors, such as the storm duration and intensity and the wind approaching direction. From this point of view, one of the most reliable experimental approaches to investigate thunderstorm-induced damage is to conduct post-event damage surveys, obtaining detailed information directly from actual damage cases to (*i*) detect damage mechanisms to different buildings and structures, (*ii*) estimate the economic losses for insurances and forensic purpose, and (*iii*) retrieve ex-post the intensity of the storm from damage observation.

Following the pioneering work by Fujita and his group (Fujita, 1971; Fujita and Smith, 1993), conventional damage surveys of thunderstorms rely on in-situ investigation. Pistotnik et al. (2011) conducted a damage survey of a remarkably intense thunderstorm downburst, with an estimated maximum wind speed of over 55 m/s, and detected severe damage to low-rise buildings such as roof and brick-wall failures due to excessive wind load. Through conducting in-situ observations and collecting witness reports (i.e., questionnaires) from more than 4000 properties (mostly low-rise buildings) in a city, Pita and Schwarzkopf (2016) identified 299 building damage cases induced by a thunderstorm downburst and a tornado, among which 32% occurred on the roofs and 39% on the facades (i.e., windows, doors/gates, wall fences). In recent years, crowdsourcing has become an alternative approach to carry out damage surveys. In addition to the direct observation of damage cases on site (Loredo-Souza et al., 2019), which is usually costly and time-consuming, the crowdsourcing approach collects the information from public sources, such as mass-media and social networking platforms (Calotescu, 2019; Calotescu et al., 2022), and/or by a group of (semi-)trained volunteers (Hao and Wang, 2020; Yuan and Liu, 2018a, 2018b).

At the current stage, there is important information regarding the thunderstorm-induced damage that has not yet been comprehensively discussed by existing survey studies. For instance, even though thunderstorms are commonly associated with hail occurrence, the damage to building envelopes induced by hailstone impacts was rarely reported in the surveys of thunderstorms. According to the European Severe Storms Laboratory, there were 6095 reported hail events with hailstone diameters over 2 cm in Europe in 2021, including 900 events with diameters of 5 cm. In 2022, the reported hail events with diameters over 2 cm increased to 9558 and those with diameters over 5 cm reached 1334, breaking the historical record. Because of such a significant amount of hail events, attention to hail-induced damage to the built environment is encouraged in survey studies. Moreover, the economic loss evaluated in most surveys focused only on insured damage, and yet the non-insured damage should not be neglected because it may occupy a considerable proportion of the total economic loss (Koks and Haer, 2020).

The possibility of detecting the intensity of severe convective weather phenomena that, due to their very localized and short-lived nature, are not usually captured by the meteorological monitoring network, is of upmost importance for regional climate analysis. The estimate of the maximum wind speed is usually derived ex-post from the resulting damage of buildings and vegetation, through an intensity rating system based on standardized scales, such as the Fujita scale (Fujita, 1971) and the enhanced Fujita scale (McDonald and Metha, 2004; Potter, 2007). However, the relationship between wind speed and damage is rather complex and the large regional variety of buildings and structures across the world hampers a globally uniform comparison of severe convective wind phenomena. The lack of comprehensive experimental support and benchmark cases, especially at the higher intensities, limits the development of an accurate model of the relation between wind speed and damage (Feuerstein et al., 2011).

Working in this field, a wide research program has been conducted in the framework of a collaboration agreement between the University of Genova, Italy (UNIGE) and the Technical University of Civil Engineering Bucharest, Romania (UTCB), establishing a long-term high-frequency continuous monitoring system on a 50 m lattice tower in Sânnicolau Mare, Romania. The location of the tower has been chosen because it is particularly prone to thunderstorm events, as resulted from previous studies related to wind-damage occurrence in Romania (Calotescu, 2019; Chitez et al., 2022). The monitoring system comprises meteorological sensors, in particular anemometer, thermometer, and sky video cameras for cloud movement detection, and structural response sensors including accelerometers and strain gauges (Calotescu and Repetto, 2022).

On June 25th, 2021, an intense thunderstorm occurred in Sânnicolau Mare, Romania, causing considerable damage to the city, due to strong wind and hailstone impact. Soon after the thunderstorm event, a survey team was dispatched to the city to collect information regarding thunderstorm-induced damage on site. Matching the high-quality monitoring records of the event and the damage survey outcomes offers a unique possibility of documenting a benchmark case of thunderstorm-induced impact on the built environment, with the aim of detecting wind-induced damage on typical buildings of the zone and verifying the capability of intensity scales of estimate the maximum wind speed. Additionally, hail-induced damage is analyzed, and novel methods are proposed to retrieve both wind intensity and direction from hail damage detection.

The paper is structured as follows: Section 2 presents the meteorological background and field measurement records of the thunderstorm events; Section 3 investigates the wind- and hail-induced damage to buildings with detailed engineering analysis on representative damaged buildings; Section 4 proposes methods to retrieve the wind field properties, i.e. the maximum wind speed and prevalent direction, using both wind- and hail-induced damage information; Section 5 summarizes the concluding remarks.

2. The thunderstorm event

2.1. Regional meteorological information

Thunderstorms originate from strong convective phenomena and are typically associated with lightning. Therefore, the trajectory of a

thunderstorm can be identified by the movement of convective cloud cells and the track of lightning strokes. As strong convections that generate thunderstorms usually produce heavy precipitation, the convective clouds can be recognized using Doppler weather surveillance radars which detect the motion of droplets. Infrared satellite images that illustrate the cloud temperatures can also be utilized for the recognition of convective clouds, as the top part of convective clouds has a very low temperature due to its high altitude. On the other hand, the track of lightning strokes can be obtained by lightning location sensors that detect the electro-magnetic pulses emitted by lightning. In this study, a variety of meteorological data of the studied thunderstorm event was collected, including the radar data provided by the National Meteorological Administration of Romania (Meteo Romania, https://www.meteoromania.ro/) as well as the infrared satellite and lightning data obtained from the Italian Civil Protection Department.

Fig. 1 (a) – (d) show the radar images for the June 25th' 2021 thunderstorm at 18:11, 18:21, 18:31 and 18:41 Coordinated Universal Time (UTC), indicating that there were convective clouds passing over Sânnicolau Mare from West to East. The meteorological system emphasized on the radar images was a mesoscale convective system known as a bow echo. Bow echoes usually begin as a single, large and strong convective cell which evolves into a bow-shaped line segment of cells, with the strongest winds occurring at the apex of the bow (Fujita, 1978). They are known to produce strong downbursts which are typically associated with damaging straight-line winds. The particular bow echo that developed on June 25th' 2021 produced a downdraft near Sânnicolau Mare with an estimated duration of 30 min. The radar images shown in Fig. 1 also indicate that the thunderstorm was accompanied by heavy precipitation. Fig. 2 illustrates the satellite image of the affected area with the locations of the lightning strokes that have occurred between 18:15 and 18:45. Notably, the track of lightning strokes passed through Sânnicolau Mare, suggesting that the city endured a direct impact by the thunderstorm.

2.2. Field measurement data

2.2.1. Monitoring systems

The full-scale field measurement data throughout the entire process of the June 25th' 2021 thunderstorm in Sânnicolau Mare were collected by two monitoring systems, namely, the wind and structural monitoring system of a lattice tower and the Sânnicolau Mare meteorological station. As indicated in Fig. 3, these two monitoring stations, located 4.7 km apart, are both within the vicinity of the urban area of Sânnicolau Mare. The distance from the lattice tower to the South-East perimeter of the urban area is approximately 1.8 km, and that from the meteorological station to the West perimeter is about 0.4 km.

The wind and structural monitoring system was established in 2021 by a research collaboration between the University of Genova (UNIGE), Italy, which is the repository of the European Research Council Advanced Grant 2016 THUNDERR (Solari et al., 2020), and the Technical University of Civil Engineering Bucharest (UTCB), Romania. Three types of meteorological data collected during the thunderstorm event were retrieved from this monitoring system for analysis, including (*i*) the horizontal wind speed and direction, (*ii*) the atmospheric temperature, and (*iii*) the video footage. The wind speed and direction were measured by a 2-axis WindObserver 70 ultrasonic anemometer (Gill Instruments, Lymington, UK), installed atop the tower at 50 m above the terrain level (a.t.l.), whereas the atmospheric temperature was measured by a PT100 transducer (F&F Filipowski, Pabianice, Poland), installed at the same height as the anemometer. The anemometer can measure the wind speed ranging from 0 to 70 m/s with a resolution of 0.01 m/s and the wind direction with a resolution of 1°. The transducer measures the temperature ranging from −50 °C to +150 °C with an accuracy of ±1 °C. The video footage, with a resolution of 1920 × 1080, was obtained by a high-definition surveillance camera (HIKVISION DS-2CE112DFT F28) orientated towards the urban area at a North – Northwest direction of approximately 335°. The time histories of wind and temperature were sampled at frequencies of 4 Hz and 10 Hz, respectively, while the camera footage was recorded at a frame rate of 15 fps.

On the other hand, the meteorological station, operated by Meteo Romania, is equipped with a variety of sensors including an ultrasonic anemometer and stores the records hourly. To understand the weather condition in Sânnicolau Mare during the thunderstorm event, this study analyzes the records of wind, temperature, air pressure, and relative humidity collected by the meteorological station. Notably, the wind records were obtained directly from Meteo Romania whilst the other records were from the National Oceanic and Atmospheric Administration database.

2.2.2. Local meteorological data

The anemometric data analyzed in this study comprises the hourly-updated data measured by the meteorological station, including the maximum 3-s gust speed and the mode of wind direction (i.e., the direction that occurs most frequently) within each hour, and the raw data sampled at 4 Hz by the wind and structure monitoring system of the lattice tower. Moreover, the air pressure and relative humidity records are also presented to provide more comprehensive meteorological information.

Based on the wind records collected by the meteorological station from 14:00 to 23:00 UTC, Fig. 4(a) and (b) show the variation of the maximum 3-s gust speed, denoted by $\hat{v}_{3,MS}$, and the mode of the wind direction, $\theta_{mode,3600,MS}$, respectively. The markers (black circles) shown in these plots correspond to the records of the previous hour, e.g., $\hat{v}_{3,MS}$ shown at 19:00 UTC represents the maximum 3-s gust speed measured

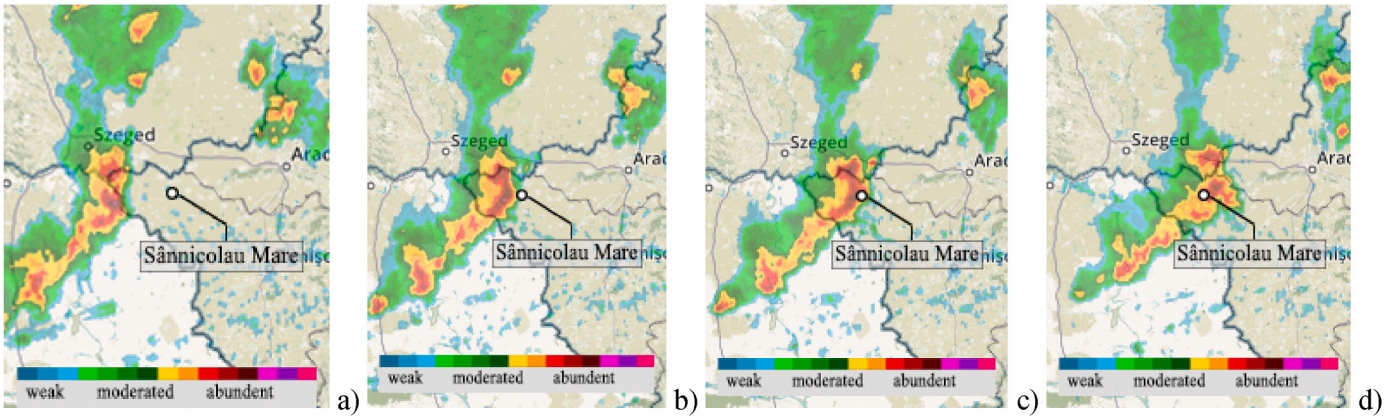

Fig. 1. Development stages of the June 25th' 2021 bow echo: radar images at (a) 18:11, (b) 18:21 and (c) 18:31 (d) 18:41 UTC images (courtesy of the Meteo Romania).

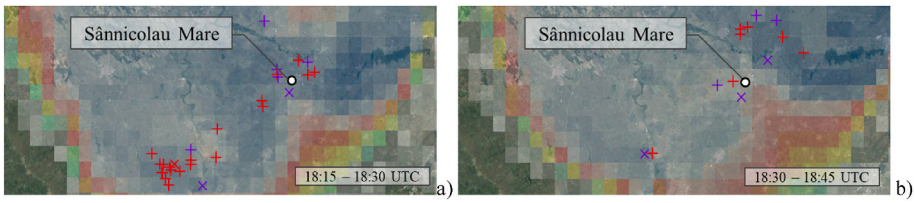

Fig. 2. Cloud movement (color-shaded area) and lightning strokes (" × " and "+" markers) over Sânnicolau Mare monitored by satellite and lightning location sensor: (a) 18:15–18:30 and (b) 18:30–18:45 UTC.



Fig. 3. Map of Sânnicolau Mare: location of the monitoring stations and of buildings A and B (Imagery ©2022 CNES/Airbus, Landsat/Copernicus, Maxar Technologies, Map data ©2022 Google).

between 18:00 and 19:00 UTC. It is readily observed that the thunderstorm resulted in a significant increase in $\hat{v}_{3,MS}$ and a noticeable variation of $\theta_{mode,3600,MS}$ during the 18:00–19:00 UTC time interval.

Fig. 4(c) presents the 3-h-long records of wind speed and direction collected by the wind and structural monitoring system from 17:00 to 20:00 UTC, which is sufficiently long to fully cover the entire passage of the thunderstorm over the city. According to these anemometric records, the instantaneous horizontal wind speed, v, stabilized at around 5 m/s for about 1 h before 18:13 UTC, and then it started to rapidly increase by approximately 35 m/s within 8 min (18:13–18:21 UTC) which is known as a ramp-up stage, followed by a gradual decrease back to 5 m/s in the next 27 min (18:21–18:48 UTC). The maximum instantaneous wind speed was $v_{max} = 40.9$ m/s recorded at 18:21 UTC, emphasizing the remarkable intensity of the thunderstorm. Notably, the time period of significant wind speed variation 18:13–18:48 UTC discussed above matches the time when the convective clouds and lightning strikes reached the city as shown in Fig. 2. As suggested by Solari et al. (2015), Fig. 4(c) also illustrates the thunderstorm intensity by the 1-s and 30-s moving mean values of wind speed, denoted by $\hat{v}$ and $\bar{v}$ respectively. Following a similar time-varying trend of v described above, both $\hat{v}$ and $\bar{v}$ also showed peak values at 18:21 UTC, i.e., $\hat{v}_{max} = 39.1$ m/s and $\bar{v}_{max} = 35.8$ m/s.

Fig. 4(d) plots the time variations of the instantaneous (θ) and 30-s moving mean ($\bar{\theta}$) wind directions measured by the wind and structure monitoring system. The wind direction is presented in a clockwise manner starting from the North, i.e., 0° and 90° denote the North and the East direction, respectively. Records show that the wind direction began to noticeably change at 18:13 UTC, which matches the starting time of the ramp-up stage as shown in Fig. 4(c), and shifted swiftly by approximately 90° from the Southwest (≈240°) to the North – Northwest (≈330°) in a clockwise manner within 15 min (18:13–18:28 UTC). After maintaining steady at the Northwest (270°–360°) for 26 min (18:28–18:54), the wind direction suddenly changed to the East (90°). It is known that the measured wind direction of thunderstorm winds is dependent on the storm-relative location of the measurement site, and hence such a significant change in wind direction as described above implies that the monitored lattice tower was located very closely to the downburst region of the thunderstorm. In general, the variations of wind speed and direction presented in this study demonstrate a typical thunderstorm process as reported in the literature (Burlando et al., 2018;

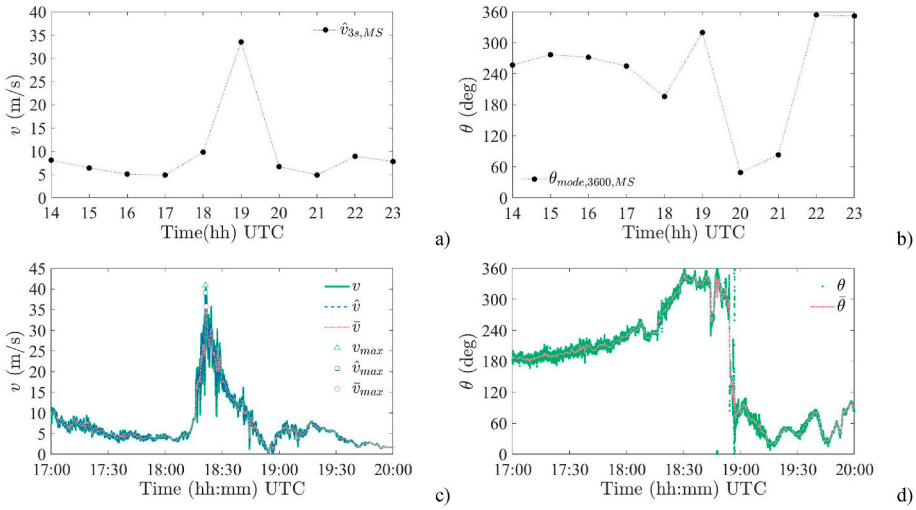

Fig. 4. Wind data recorded by the meteorological station (data provided by Meteo Romania): (a) maximum 3-s gust speed and (b) mode of wind direction and by the monitoring system installed on the telecommunication tower: (c) wind speed and (d) wind direction.

De Gaetano et al., 2014; Solari et al., 2015).

To further investigate the wind characteristics of the outflow winds, the wind velocity decomposition approach (Choi and Hidayat, 2002; Solari et al., 2015) is adopted in this study, expressed as follows:

$$v(t) = \overline{v}(t) + v'(t) \tag{1}$$

where t is the time, $\overline{v}$ is the slowly varying mean wind velocity extracted using a 30-s moving average filter (Solari et al., 2015), and v' is the residual fluctuation given by:

$$v'(t) = \sigma_v(t)\widetilde{v}'(t) \tag{2}$$

where σ_v is he slowly-varying standard deviation of v', and $\widetilde{v}'$ is the reduced turbulent fluctuation.

By replacing Eq. (2) into Eq. (1), the wind velocity can be expressed by:

$$v(t) = \overline{v}(t)[1 + I_v(t)\widetilde{v}'(t)] \tag{3}$$

where I_v represents the slowly-varying turbulence intensity expressed as:

$$I_v(t) = \frac{\sigma_v(t)}{\overline{v}(t)} \tag{4}$$

By decomposing the 1-hr-long wind velocity record centered at v_{max} following the approach introduced above, the variations of v, $\overline{v}$, v', I_v, and $\widetilde{v}'$ with time are presented in Fig. 5(a)–(f), respectively. It is readily observed that $\widetilde{v}'(t)$ was non-stationary and reached the maximum value of 6.05 m/s at the same time instant when v_{max} occurred. On the other hand, the mean value of I_v was 0.074 within the 1-hr time interval.

Fig. 6(a) shows the 9-h-long temperature data recorded at the monitored lattice tower and the meteorological station, denoted by T and T_{MS} respectively, from 14:00 to 23:00 UTC. Records show that T decreased gradually by 6.7 °C in more than 4 h (14:00–18:16 UTC) and then suddenly dropped by 12.5 °C within only 12 min (18:16–18:28 UTC), followed by a relatively moderate increase. Such abrupt decrease in temperature occurred almost simultaneously with the rapid increase in wind speed depicted in Fig. 4(a), demonstrating the typical feature of a thunderstorm that the downdraft transported cool air from the cloud to the ground. It is noted that T_{MS} collected at the meteorological station are generally in good agreement with T measured at the lattice tower, validating the accuracy of the temperature measurement by the wind and structure monitoring system. Fig. 6(b) shows the hourly-updated data of air pressure and relative humidity recorded at the meteorological station from 14:00 to 23:00. Both parameters significantly varied around 18:00, i.e., the air pressure increased from 1010.0 hPa to 1012.6 hPa and the relative humidity boosted from 48% to 100%, suggesting that precipitations occurred during the thunderstorm event.

2.2.3. Video surveillance data

Whilst most field measurement studies of thunderstorms conducted over the past decades were based only on anemometric data, the wind and structure monitoring system of the lattice tower adopted innovative vision-based techniques, recently used in meteorological and energy sector (Beekmans et al., 2021), to improve the capability of detecting thunderstorms from sky-imaging data. Although the visual information may not offer quantitative data, it provides useful observations such as the structure of a thunderstorm cloud (i.e., cumulonimbus) and the period of precipitation that cannot be reflected by anemometric data. Fig. 7 presents three frames extracted from the footage, and the time stamp of each frame refers to the local time which is equivalent to UTC +3 h (e.g., 21:00 local time = 18:00 UTC).

As shown in Fig. 7(a), the frame taken at 18:15 UTC (21:15 local time) demonstrates several typical features of a thunderstorm including the storm cell, the lightning strokes, and the heavy precipitation. The

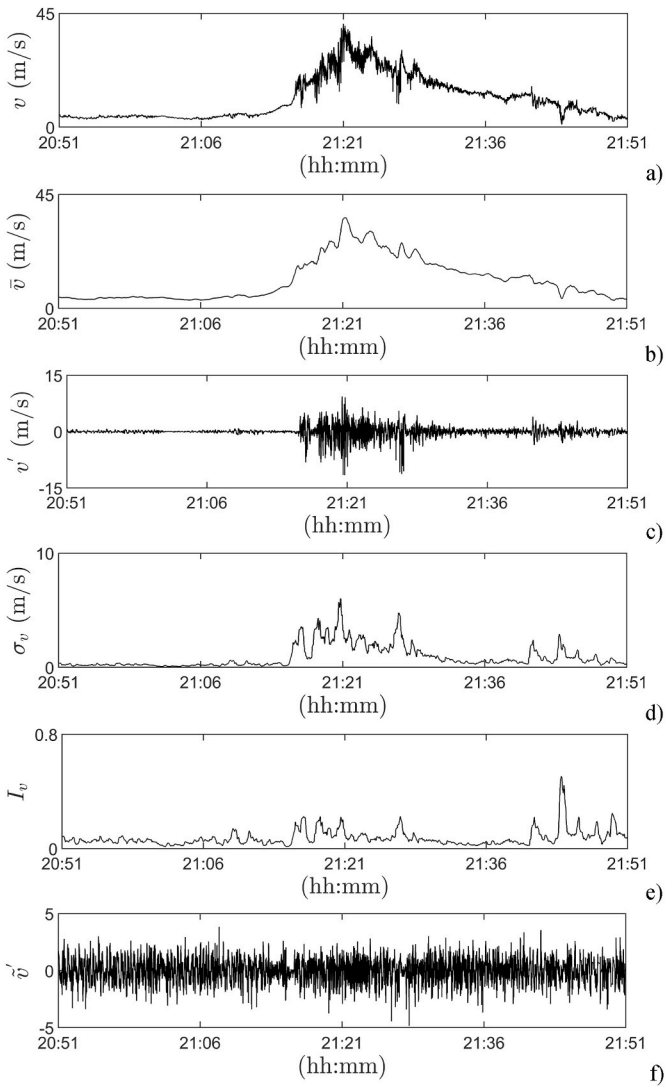

Fig. 5. Wind velocity decomposition of the June 25th, 2021 record: (a) v; (b) $\overline{v}$; (c) v'; (d) σ_v; (d) I_v; (f) $\widetilde{v}'$.

cloud movement indicates that the thunderstorm motion (also known as translation) towards the urban area was from the West, coinciding with the radar and satellite images presented in Figs. 1 and 2, respectively. However, the crops bent by surface wind suggested that the boundary layer (background) flow near the telecommunication tower was approaching from the Southwest, which agrees with the anemometric records shown in Fig. 4. Such observed difference in direction between the storm motion and the boundary layer wind indicates that there is a clear distinction between the translational velocity and the background velocity as pointed out in literature (Xhelaj et al., 2020). According to the significant change in the direction of surface wind shown in Fig. 7 (b), the thunderstorm outflow reached the telecommunication tower at 18:18 UTC (21:18 local time). It is also noted that the precipitation over the urban area started around the same time. At 18:22 UTC (21:22 local time), as presented in Fig. 7(c), the surface wind near the telecommunication tower approached from the direction of the urban area, implying that the storm cell was directly above the urban area at that time. Moreover, the video camera images also emphasize the size of the downburst which is comparable to the size of the city. This suggests that the intensity of wind-induced damage to the built environment throughout the city is relatively similar.

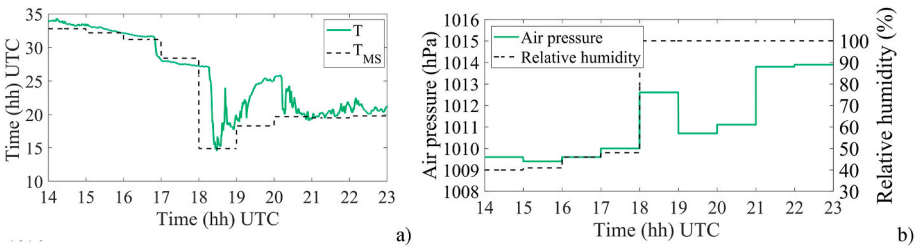

Fig. 6. Meteorological data: (a) atmospheric temperature and (v) air pressure and relative humidity.

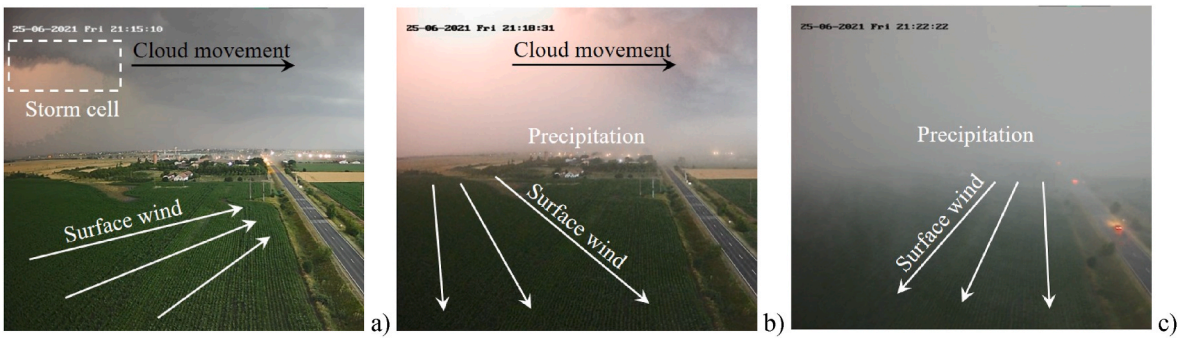

Fig. 7. Video camera images showing cloud movement at different times (UTC): (a) 18:15; (b) 18:18; (c) 18:22.

2.3. Wind speed profile model

It is known that the wind-resistant design of structures is based on the assumption that the wind profile follows a power or logarithmic law for synoptic boundary layer winds, and such assumption is obviously inapplicable in the case of thunderstorm outflow winds which follow a nose-shape profile. Therefore, a comparison is made herein to demonstrate the difference in the estimated wind speed obtained by the two different profiles, and to discuss the potential risk of unconservative wind-resistant design of structures against thunderstorms. The wind speed of a thunderstorm outflow is usually expressed as a composition of the slowly-varying mean wind speed and the residual fluctuation (Eq. (1)), which relate to the low and high frequency contents of wind speed, respectively (Chen and Letchford, 2004; Choi and Hidayat, 2002). Field observations reported that the slowly-varying mean wind speed of a thunderstorm significantly varies with height following a "nose-shaped" profile, that is, the speed first increases with height, reaches the maximum value at a certain height above ground, and decreases afterward. One of the most commonly used wind speed profile models of thunderstorm outflow was proposed by Wood et al. (2001) based on the experimental results of an impinging jet, expressed as:

$$\frac{U(z)}{U_{\max}} = 1.55\left(\frac{z}{\delta}\right)^{\frac{1}{6}}\left[1 - erf\left(0.70\frac{z}{\delta}\right)\right] \tag{5}$$

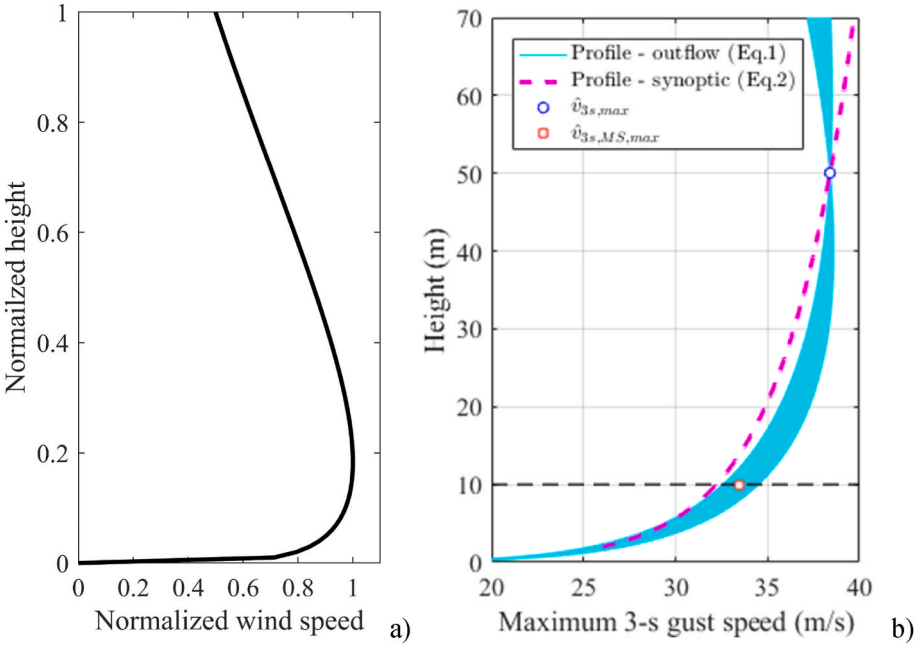

Fig. 8. Horizontal wind speed profiles of thunderstorm outflow: (a) normalized wind speed; (b) maximum 3-s gust speed.

where $U(z)$ denotes the slowly-varying mean wind speed (in m/s) at the height z (in m) over the terrain level, U_{max} denotes the maximum value of the slowly-varying mean wind speed occurring at the height z^*, δ denotes the height above z^* where the slowly-varying mean is equal to 0.5 U_{max}, and erf[.] is the error function.

Fig. 8(a) shows the wind speed profile expressed by Eq. (5) by plotting the normalized wind speed, $U(z)/U_{max}$, against the normalized height, z/z^*. The anemometric records collected at different heights at these two measurement sites are compared with the outflow profile model proposed by Wood et al. (2001). According to the video footage and radar data collected during the thunderstorm event, the monitored tower and the meteorological station were both swept by the outflow fronts (i.e., winds with the maximum intensity) during the thunderstorm event. Such observation coincides with previous field measurement studies that the thunderstorm outflow fronts usually sweep over an area 5–7 km in diameter (Hjelmfelt, 1988). Therefore, in the absence of more accurate measurements, it is reasonable to believe that the outflow winds over these two sites followed a similar profile. In this study, it is assumed that the 3-s gust speed profile follows the same shape of mean wind speed profile in Eq. (5) at near-surface height. Records showed that the maximum 3-s gust speed atop the telecommunication tower, denoted by $\widehat{v}_{3,max}$ herein, was 38.4 m/s at 50 m height. Given that z^* ranges from 40 to 60 m above ground according to the field study conducted by Hjelmfelt (1988), Fig. 8(b) shows the profiles of maximum 3-s gust speed following Eq. (5) using different values of z^*, and these profiles lead to an estimated $\widehat{v}_{3,max}$ ranging from 32.6 to 34.5 m/s at 10 m height. Meanwhile, the maximum 3-s gust speed collected by the meteorological station at 10 m height, $\widehat{v}_{3,MS,max}$, was 33.5 m/s, which falls within the range of the estimated $\widehat{v}_{3,max}$ at the same height as shown in Fig. 8(b). The good agreement between the estimated $\widehat{v}_{3,max}$ by Eq. (5) and the measured $\widehat{v}_{3,MS,max}$ suggests that the empirical wind speed profile model proposed by Wood et al. (2001), according to the measurement data of this study, may be applicable to model the actual thunderstorm outflows. Nevertheless, it is noteworthy that such statement is associated with uncertainties, because value of z^* in this study was obtained from Hjelmfelt (1988) rather than measured directly during the monitored thunderstorm event.

Furthermore, the measured wind speed is also compared with the synoptic wind speed profile model proposed by structural design codes. In the Romanian wind code (CR1-1-4, 2012), which is essentially an adapted version of the Eurocodes (EN1991-1-4, 2005), the profile of gust speed is expressed following a logarithmic law as below:

$$v_p(z) = [1 + gI_v(z)]k_r(z_0)\ln\left(\frac{z}{z_0}\right)v_b \tag{6}$$

where z denotes the height above ground level, $v_p(z)$ denotes the gust speed at height z, g denotes the peak factor that is dependent on the duration of gust and the averaging interval of mean wind speed (Solari, 1993), $I_v(z)$ denotes the along-wind turbulence intensity at height z, k_r denotes the factor that reflects the terrain condition (suburban terrain for Sânnicolau Mare), z_0 denotes the roughness length, v_b denotes the 10-min reference wind speed at 10 m a.t.l. corresponding to a mean recurrence interval of 50 years and it equals 25.25 m/s for Sânnicolau Mare.

Following Eq. (6), the 3-s peak wind speed at 10 m a.t.l is $v_p(10) =$ 40.1 m/s and that at 50 m a.t.l. is $v_p(50) = 47.8$ m/s, showing that the maximum wind speed in the actual event is covered by the Code recommendation. $v_p(50)$ Through scaling Eq. (6) to the wind speed measured at 50 m a.t.l. the corresponding 3-s gust speed at 10 m a.t.l., $v_p(10)$, is slightly lower than the value measured by the meteorological station, suggesting that the synoptic wind speed profile may result in an underestimation of wind speed during thunderstorm events at near-surface heights.

3. Analysis of thunderstorm-induced damage

3.1. Post-event damage survey

To fully investigate the thunderstorm-induced damage in the city, a joint research group from the UNIGE and the UTCB was deployed to conduct a post-event damage survey. The survey employed a dual approach combining the in-situ investigation and crowdsourcing: the former collects damage data in detail by observations on site, whereas the latter collects information from various sources on the internet as a supplement to the former. The in-situ investigation commenced on July 7th, 2021 and lasted for 4 days, and the crowdsourcing began immediately after the thunderstorm event.

To collect comprehensive information regarding the thunderstorm-induced damage to the built environment, the survey covered the entire urban area of Sânnicolau Mare (highlighted area in Fig. 3), which is approximately 8.5 km^2 in size. According to the 2011 population census ("Romanian National Institute of Statistics," 2011), there are over 2000 structures in the surveyed area with a majority of single-story residential buildings. Witness reports were also collected from the habitants who experienced the thunderstorm event, providing credible descriptions of the damage cases such as the process and the time of occurrence. On the other hand, crowdsourcing retrieved data that are publicly available on social networking platforms and broadcast media websites. These crowdsourced data, including photos/videos and texts, were carefully examined and cross-validated to guarantee that they originated from the exact thunderstorm event discussed in this study. Through the dual approach introduced above, this study identified 237 thunderstorm-induced damage cases of low-rise buildings. Notably, the damage cases reported herein were either publicly available (i.e., observable without privacy violations) or collected with the consent of property owners.

3.2. Observed wind-induced damage

Despite the remarkable intensity of the thunderstorm, the in-situ investigation shows that the vast majority of the civil structures in the urban area only suffered low and medium wind-induced damage. Among the few severe wind-induced damage cases, the building roofing system failure was the most common damage type. A total number of 17 roof damage cases were collected in this study, including four cases observed on site and 13 identified by crowdsourcing. It is noteworthy that there might be more wind-induced roof damage cases according to the witness reports, but these extra cases were not verified by the survey team (due to limited accessibility to private properties) and therefore they are excluded in this paper to ensure the data accuracy. All of the damage cases were observed from gable or hip roofs, which are the two most common roof shapes in the surveyed area. Fig. 9 shows the locations of damaged building roofs, including 10 cases in the city center and five cases near the perimeter of the urban area. All of the roofs sustained moderate wind-induced damage with less than 20% loss of roof covering material.

There were two types of damaged roofs in terms of roofing materials, namely, 10 sheet metal roofs and 7 clay tile roofs. Due to the small sample size, this study has no intention to compare the wind-resistant performances of these two roofing materials. Fig. 10 presents a site photo of each type of damaged roofs, and the loss of roofing materials can be observed with ease. This pattern of wind-induced roof damage during the thunderstorm is similar to that during tropical cyclones as reported in previous field survey studies (Meloy et al., 2007).

Among the building damage cases induced by the destructive thunderstorm winds, the most severe was observed from a church building, referred to as "Building A" herein, which is located 3.4 km Northwest from the monitored lattice tower as shown in Fig. 2. According to the interview with the personnel in charge of the restoration, the damage to Building A led to a direct economic loss of approximately 50,000 Euros

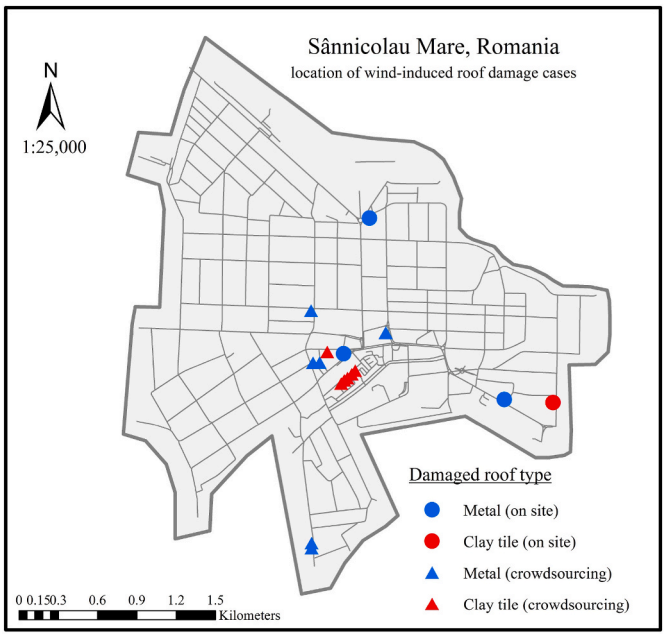

Fig. 9. Locations of wind-induced roof damage cases.

(currency rate at the occurrence time of the thunderstorm). Given the extent of the wind-induced damage to Building A, a thorough in-situ investigation of this building was conducted to reveal the damage mechanisms, so as to provide practical suggestions to the wind-resistant designs of similar structures. It can be observed from Fig. 11 that Building A, as a typical church building, comprises a hall on the Southwest side and a bell tower attached to the Northeast end of the hall. Both the hall and the bell tower are covered by sloped sheet metal roofs with the mean roof heights (i.e., mean of the top and bottom heights of a sloped roof) of approximately 18 and 25 m, respectively. It is noteworthy that the structures in the proximity of Building A, as shown in Fig. 11(a), are generally below 15 m in height and located at least 15 m away, and therefore the wind shielding effect on the roofs of Building A provided by them are negligible. Fig. 11(b) and (c) present the site photos of Building A before and after the thunderstorm event, respectively, and significant roof damage can be observed with ease by comparison.

In-situ investigation shows that the wind-induced damage of Building A has mainly occurred in four areas, denoted by Areas I to IV in Fig. 12(a), including three areas of major roof damage and one of window damage. The most significant roof damage was found in Area I, where the sheet metal roof of over 500 m^2 in area was almost entirely removed from the building as presented in Fig. 12(b). The western edge of the roof in Area I-A was detached from the lower structure (i.e., battens or rafters) while the roof in Area I–B fell to the ground approximately 20 m East from its original location, suggesting that the



Fig. 10. Site photos of wind-induced roof damage: (a) sheet metal roof and (b) clay tile roof.

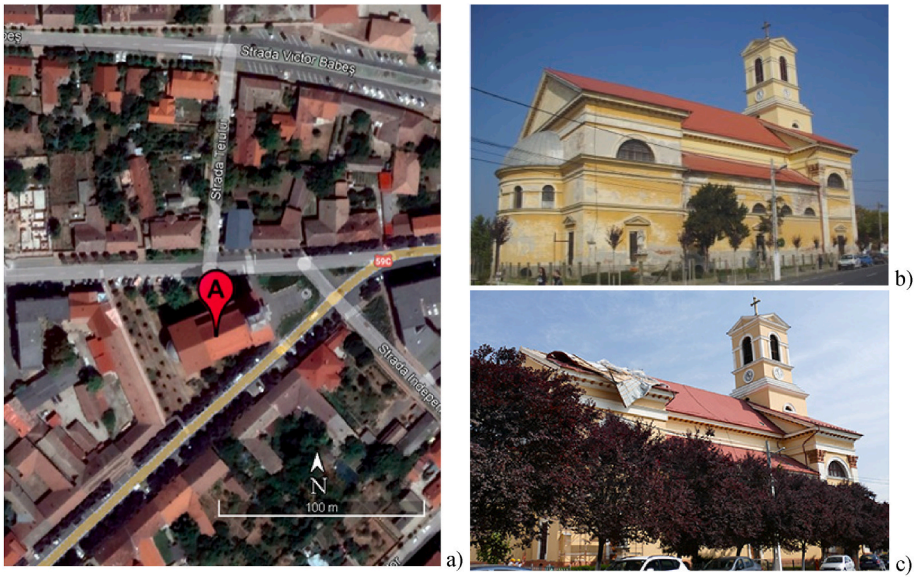

Fig. 11. Building A (Imagery ©2022 CNES/Airbus, Maxar Technologies, Map data ©2022 Google: (a) location, (b) building before damage (©2022 Google) (c) wind-induced roof damage.

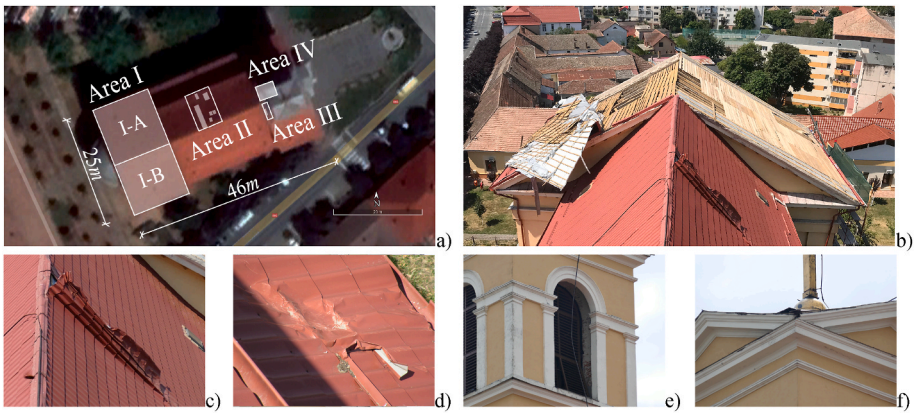

Fig. 12. Wind-induced damage to Building A: (a) top view and damage areas; (b) roof damage in Area I (partially restored); (c–d) roof damage in Area II; (e) window damage in Area III; (f) roof damage in Area IV.

damaged roof in this area was uplifted by the winds approaching from the West. Such inference of the wind direction based on forensic analysis aligns with the meteorological data presented in Section 2 that the thunderstorm outflow approached the urban area from the West. Since there was no opening on the facades of the hall to allow the wind flows to enter, it is evident that the roof failure in Area I was initiated mainly, if not solely, by the excessive suction force that occurred at the roof edge on the west side due to flow separation. The site photos shown in Fig. 12 (c) and (d) demonstrate multiple indentations observed from the roof in Area II. Evidence such as the debris found on the scene suggested that these indentations were caused by the roofing materials in Area I–B, which became wind-borne debris after their detachment from the lower structure and impacted the roof in Area II during the falling process. Notably, the close-up inspection showed no sign of penetration through the roof in Area II, indicating that the roof in this area remained functional for the sheltering purpose throughout the thunderstorm event. Fig. 12(e) shows that the wooden louver window on the west facade of the bell tower, referred to as Area III, was displaced inward for approximately 30 cm, whilst no damage was observed from an identical window closely located on the North facade. Obviously, such window damage resulted from the excessive positive pressure induced by the thunderstorm outflow approaching from the West. Approximately 2 m above the damaged window, the roof of the bell tower near the Northwest corner, denoted by Area IV, was also uplifted during the thunderstorm event as demonstrated in Fig. 12(f). The roof damage in Area IV could be attributed to both the negative external pressure, which was generated by the flow separation at the roof edge/corner, as well as the positive internal pressure, which was boosted by the wind flows entering through the windows.

3.3. Observed hail-induced damage

Formed in the clouds of an intense thunderstorm, hailstones may induce damage to the envelope (i.e., roof and facades) of a civil structure upon impact, provided that their kinetic energy gained from the fall and the wind is adequate. Over the past few decades, the knowledge of hail-induced damage to building roofs has advanced significantly, and the hail-resistant capability of roofing materials is usually stipulated in most design standards/codes. However, information regarding the hail-induced damage to building facades is still lacking, probably because the facades are not expected to endure hailstone impacts. However, due to the strong horizontal winds during thunderstorm events, the trajectories of hailstones are likely to deviate from the vertical direction and may lead to hailstone impacts on building facades. Through in-situ investigation, a total number of 220 facade damage cases induced by hailstone impacts during the thunderstorm event were identified, and such significant damage needs to be properly considered in hail-resistant building designs.

Site photos of typical hail-induced facade damage to a single-level residential building are presented in Fig. 13, from which the indentations caused by hailstone impacts can be observed from both the window shutters (Fig. 13(b)) and the thermal insulation layers (TILs) (Fig. 13(c)) adhered to the exterior walls. The isolated indentations on window shutters ranged from 0.5 to 1.5 cm in diameter, whilst those on TILs were between 0.5 and 3.0 cm. In general, the indentations on TILs appeared to be larger in size, which is reasonable because the TILs are softer than the window shutters made of aluminum alloy. Based on the indentation size observed from the building facades, it is inferred that the maximum diameter of hailstones, denoted by D herein, was approximately 3.0 cm during the thunderstorm event. Such inference of D matches both the description by a witness, who also provided a photo of hailstones taken about 12 h after the event as proof (Fig. 13(d)), and the report released by the European Severe Storms Laboratory (https://eswd.eu/), which recorded $D = 3$ cm at around 18:30 UTC. In comparison with the statistics reported in previous studies based on historical data, the observation of $D = 3$ cm coincides with $D \in [4, 6]$ cm reported in Punge and Kunz (2016) and exceeds $D \in [1.5, 2]$ cm in Burcea et al. (2016), indicating that the hailstone size observed in this survey was one of the largest in the local area.

In this survey, approximately 90% (i.e., 197/220) of the hail-induced facade damage cases were observed from TILs. Comparing with the damage to other parts of a building facade (e.g., window shutters), that to the TILs affects the habitability of a building to a much larger extent because it worsens the performance of the thermal insulation system. In-situ investigation showed that the damage intensity to a TIL was highly dependent on its render. The structure of a complete TIL render consists of a base coat and a top coat, whereas in practice the top coat may be omitted and the base coat is exposed to the external environment. Fig. 14 shows the damage to both complete (with top coat) and incomplete (without top coat) TILs, and it is observed with ease that the damage intensity to the incomplete TIL was evidently higher. It was also found that, although only 21% of the TILs in the surveyed area were incomplete (estimated from 405 randomly sampled facades), 68% (135/197) of the damage cases were observed from the incomplete TILs. Hence, in the case of this survey, the probability of an incomplete TIL suffering hail-induced damage was 7.9 times that of a complete TIL.

Fig. 15 shows the examples of hail-induced facade damage of four representative single story residential buildings located in different areas of the city. All facades are oriented towards the West, which was the approaching direction of the outflow. Facades 1 and 2 (Fig. 15(a)and (b)) are representatives of the TIL with top coat category whereas Facades 3 and 4 (Fig. 15(c)and(d)) belong to the TIL without top coat category. Although Facade 1 and Facade 2 belong to buildings that are closely located (only 130 m apart), Facade 1 showed considerable



Fig. 13. Typical hail-induced facade damage: (a) damaged facade; (b) indentations on window shutter; (c) indentations on thermal insulation layer and (d) hail (photo taken about 12 h after the event).

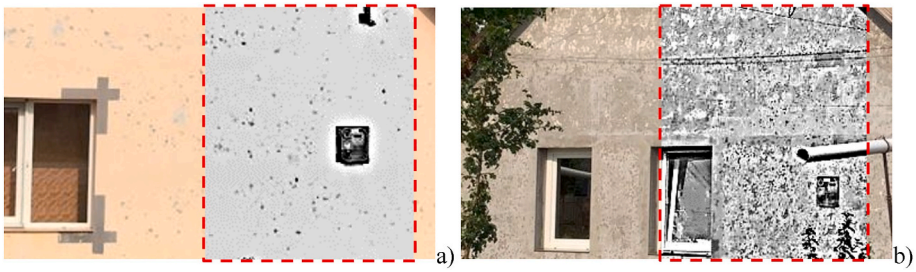

Fig. 14. Hail-induced damage to TILs: (a) TIL with top coat; (b) TIL without top coat.

damage over approximately 90% of the facade area, whereas damage on Facade 2 was barely noticeable, at a level of less than 5%. On the contrary, Facades 3 and 4, located approximately 200 m apart, showed very similar damage patterns.

To investigate the hail-induced TIL damage more comprehensively, this study selects a 10-m-tall three-story building, referred to as "Building B″ herein, which is located 3.7 km Northwest to the telecommunication tower as shown in Fig. 3, for detailed forensic engineering analysis. The facades of this building, located perpendicularly or parallelly to each other, are orientated along the North-South or the East-West directions. Building B is located in a relatively open area: there are no obstacles on the West and East sides of this building for over 25 m, while the neighboring structures with heights below 7 m on the North and South sides of Building B are located more than 9 m away. Hence, it is believed that the facades of Building B were fully exposed to the winds, as well as the hailstones driven by the winds, during the thunderstorm event. Fig. 16 presents a site photo of Building B, demonstrating numerous hail-induced indentations with diameters from 0.5 to 3.0 cm on its incomplete TILs. Notably, these indentations were mostly observed from the West facade whilst almost none was found on the North facade (or the two other facades not shown in Fig. 16). Such observation coincides with the statement above that the orientations of damaged facades are strongly correlated with the outflow direction. The in-situ investigation also found that the small areas beneath the eave and the balconies, as shown in the close-up view in Fig. 16, were not damaged by the hailstone impacts. By correlating the depths of balconies and the heights of undamaged areas beneath, it is calculated that the attack angle (denoted by α in Fig. 16) of the hailstones was approximately 45°, and such a low attack angle reflects the remarkable wind force that drove the hailstones horizontally. Moreover, a close inspection of the damage around corners shows that less damage is present around the external corner (Fig. 16(a)) than around the internal corner (Fig. 16(c)) of the building. Budlings presented in Fig. 15 showed similar patterns.

To discuss the hail-induced damage to Building B quantitatively, this study evaluates the damage intensity by the number of indentations per area. Fig. 17(a) shows the damaged TIL on the West facade (middle part) of Building B. Through processing the high-resolution photo as shown in the figure, over 8000 indentations on the TIL are identified accurately. Fig. 17(b) illustrates the distribution of damage intensity on the TIL using a square grid, of which each square is 30 cm × 30 cm (or equivalently, 1 ft × 1 ft) in size following the dimensions of a standard hail



Fig. 15. Hail-induced damage patterns: (a) Facade 1; (b) Facade 2; (c) Facade 3 and (d) Facade 4.



Fig. 16. Hail-induced TIL damage to Building B: (a) general view and corner details: (b) convex and (c) concave.

pad utilized in previous field surveys (Palencia et al., 2007). The damage intensity on the TIL increases evidently with height, given that the number of indentations per 900 cm^2 (1 ft^2) increases from below 10 within the bottom area (below 1.5 m in height) of the TIL to over 25 within the top area (above 7.5 m). It is known that the wind speed at near-ground level (say below 10 m above ground) also increases with the height, and therefore such observation of TIL damage intensity implies the existence of a strong correlation of the intensity of hail-induced damage with the wind speed.

3.4. Estimation of economic loss

Based on the observed wind- and hail-induced damage to buildings specified in Sections 3.2 and 3.3, respectively, the present study evaluates the thunderstorm-induced economic loss according to the costs of materials and workmanship needed for repairment in Romania. The most recent cost standards elaborated by the Romanian Ministry of Development, Public Works and Administration for construction works were approved in 2010 (MDLPA, 2010), which include cost estimates for specific typologies of buildings such as blocks of flats, cultural centers, schools, and hospitals, providing overall construction costs. As discussed

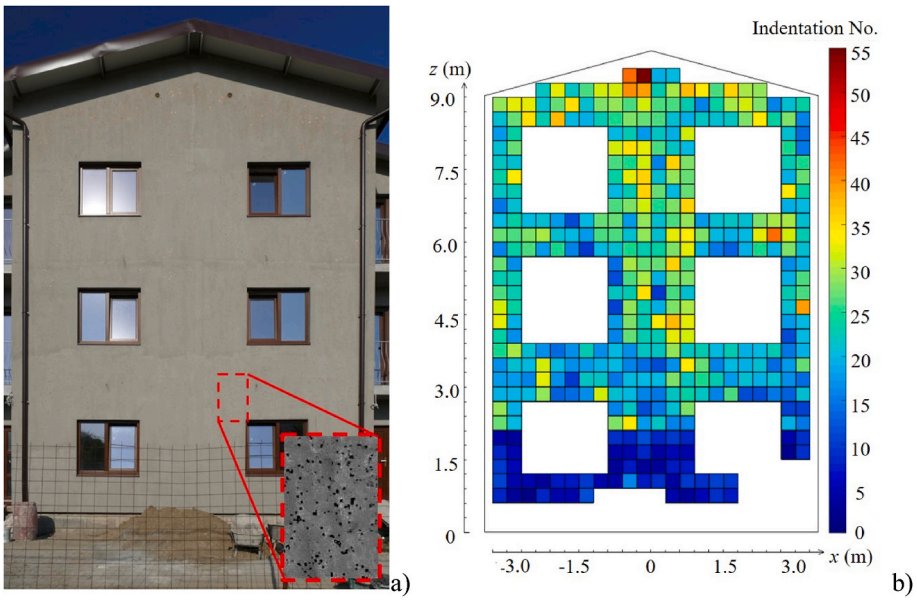

Fig. 17. Hail-induced TIL damage to the West facade (middle part) of Building B: (a) high-resolution photo of TIL; (b) distribution of hail damage intensity.

above, the wind- and hail-induced damage were mostly observed from roofs and the TILs, respectively, and hence the economic loss corresponding to these two types of damage are evaluated herein.

For the wind-induced roof damage, since the official cost estimates are not available in Romania, this study evaluates the corresponding economic loss based on offers from construction companies, which is 75 Euros/m^2. Considering the affected areas of the damaged roofs identified during the damage survey (blue circles in Fig. 9), a total estimated repair cost of 15,000 Euros is obtained to which the church repairment cost is added amounting to 65,000 Euros. The roofs identified by crowdsourcing were not taken into account for the estimation of the economic loss.

On the other hand, to estimate the cost of hail-induced damage to TILs, the 2012 cost standard for thermal rehabilitation of blocks of flats SCOST-04/MDRT (MDLPA, 2010) may be used. The standard estimates an overall cost of 34 Euros/m^2 (as in 2010), which includes materials, transportation, labor, indirect costs, and profit. Considering that the buildings with damaged TILs are typically one- or two-story residential buildings and that the extent of damage would need repairment only for the damaged parts, a repairment cost of 30 Euros/m^2 is estimated based on offers received from construction companies. From the 197 TIL damage cases, statistics indicated that the damaged TIL parts of a building generally ranged from 30 to 60 m^2 in size, which leads to a rough estimate of overall hail-induced economic loss of 300,000 Euros.

4. Wind field retrieval from damage survey

4.1. Wind intensity retrieval from wind-induced damage

The intensity of a wind event can be estimated based on the wind-induced damage observed in the post-event survey. This study employs four widely adopted wind speed estimation scales, namely, the Fujita scale (Fujita, 1971) abbreviated as F-scale herein, the enhanced Fujita scale (McDonald and Metha, 2004; Potter, 2007) abbreviated as EF-scale, the Canadian EF-scale (Environment Canada, 2022) and the Japanese EF-scale (Japan Meteorological Agency, 2015). Although these scales were initially proposed for estimating the intensity of tornadoes, they were also implemented for other extreme wind events such as tropical cyclones in literature (Powell and Houston, 1996). Notably, the EF-scales estimate the maximum 3-s gust speed at 10 m height during the wind event, whilst the wind speed estimated by the F-scale refers to the fastest one-quarter mile speed and is converted to the maximum 3-s gust speed using the Durst curve (Durst, 1960) in this study.

The survey results showed that the loss of roofing materials in the majority of damage cases (not including Building A) was below 20%, which is categorized as a moderate damage by the F-scale and a degree of damage 2 by the three EF-scales. Table 1 summarizes the maximum 3-s gust speeds estimated by the four scales according to the observed damage to buildings. For the EF-scale estimates shown in Table 1, the values outside the brackets are the expected speed under "normal" structural conditions of the buildings (i.e., no glaring weak links, traditional construction quality, appropriate building materials, compliance with local building code, and continuous maintenance), and the values inside the brackets refer to the wind speed ranges accounting for circumstances that cause the actual wind speed to deviate from the expected value (McDonald and Metha, 2004). For validation purposes, the wind speeds estimated by the F-scale and EF-scales are compared with $\widehat{v}_{3,MS,max}$ m/s measured by the meteorological station. Results show that $\widehat{v}_{3,MS,max}$ falls within the wind speed range estimated by F-scale (32.6–50.1 m/s) but is only slightly above the lower bound wind speed. Comparing with the F-scale, the EF-scales appear to estimate the wind

Table 1
Gust speeds estimated by F-scale and EF-scales.

Scale and damage indicator	Damage description	Estimated maximum 3-s gust speed
Fujita (F): F1	Moderate damage: roof surfaces peeled off; mobile homes pushed foundations or overturned; moving autos pushed off road.	32.6–50.1 m/s
Enhanced Fujita (EF): One- and two-family residence	Degree of damage 2: Loss of roof covering material (<20%), gutters and/or awning; loss of vinyl or metal siding	35.3 (28.6–43.4) m/s
Canadian EF: One- and two-family residence, 100–500 m^2	Degree of damage 2: Loss of roof covering material (<20%), gutters and/or awning; loss of vinyl or metal siding	34.7 (27.8–43.1) m/s
Japanese EF: Wooden houses and stores, 1 or 2 stories	Degree of damage 2: Minor loss (detachment)/displacement of roofing materials: clay tile (CT) and sheet-metal (SM)	35 (25–50) m/s for CT 40 (30–55) m/s for SM

intensity at a higher accuracy. The expected maximum 3-s wind speeds estimated by the EF-scale (35.3 m/s), the Canadian EF-scale (34.7 m/s), and the Japanese EF for buildings with clay tile roofs (35 m/s) all agree well with $\widehat{v}_{3,MS,max}$.

4.2. Wind intensity retrieval from hail-induced damage

Although the hail phenomenon commonly occurs during a thunderstorm event, the hail-induced damage has not yet been adopted for the estimation of wind speed in most scales including the F-scale and EF-scales. Based on forensic engineering analysis, this study explores the correlation between the hail-induced damage to TIL and the wind speed, so as to investigate the feasibility of utilizing such damage type to estimate the storm intensity. Essentially, the hail-induced damage to TIL is the consequence of an energy conversion process, i.e., from the kinetic energy of the hailstones to the deformation of the facade impacted by these hailstones. To achieve the hail-induced TIL damage observed from Building B, the experiments conducted by Francke and Zamorowska (2020) suggested that the kinetic energy of a hailstone, denoted by E_k herein, is within the range from 3 to 10 J at the time instant of impact. As suggested by Paterson and Sankaran (1994), the impact force of a hailstone applied to a vertical surface (i.e., facade) is related solely to the horizontal component of the hailstone speed. Since the attack angle of the hailstone impacts on Building B was approximately 45° as discussed above (Fig. 17), it is inferred that the horizontal speed component was similar to the vertical component in terms of magnitude, and thus the vertical speed of a hailstone also corresponds to $E_k \in [3, 10]$ J.

Following the field observations of hailstone impacts on horizontal surfaces reported in literature, the kinetic energy of a hailstone is size-dependent and can be empirically expressed by a power-law as follows:

$$E_k = aD^b \tag{7}$$

where E_k denotes the kinetic energy in J, D enotes the maximum diameter of a hailstone in cm, and a and b are the curve-fitting constants. Two widely used empirical models are selected in this study, namely, [$a = 0.0406$ and $b = 4.02$] proposed by Laurie (1960) and Waldvogel et al. (1978), and [$a = 0.0458$ and $b = 4.00$] proposed by Schmid et al. (1992). Notably, the values of curve-fitting constants of the first model are obtained from Heymsfield et al. (2018). As illustrated in Fig. 18(a), these two models suggest very similar estimates that to $E_k \in [3, 10]$ J corresponds to $D \in [2.9, 3.9]$ cm, which generally agrees with the hailstone diameter of 3 cm reported in the survey as discussed above.

Given the size of a hailstone, its terminal speed, i.e., the maximum and final vertical speed before impact, can be obtained empirically by:

$$V_t = cD^d \tag{8}$$

where V_t denotes the terminal velocity in m/s, and $c = 13.95$ and $d = 0.51$ are the curve-fitting constants suggested by Laurie (1960).

Fig. 18(b) presents the correlation between V_t and D demonstrating that the hailstones in the size of $D \in [3, 4]$ cm correspond $V_t \in [24.0, 27.9]$ m/s. Therefore, it is estimated that the horizontal speed of hailstones, which had around the same magnitude of V_t as discussed above, was also approximately [24.0, 27.9] m/s during the studied thunderstorm event. According to Paterson and Sankaran (1994), the mean horizontal speed of a hailstone is equal to the horizontal mean wind speed, suggesting that the hailstones were driven by the winds at a mean speed of approximately [24.0, 27.9] m/s when they impacted Building B. On the other hand, by adopting the wind speed profile of thunderstorm expressed by Eq. (5), the mean wind speed at the roof height of Building B (i.e., 10 m above ground) can be estimated from the anemometric records collected at 50 m in height. As stated in Section 2.2, the precipitation over the urban area driven by westerly winds lasted from 18:18 to 18:22 UTC, over which period the mean wind speed collected by the anemometer was 25.8 m/s. Following Eq. (5), it is estimated that the mean wind speed at 10 m above ground was [21.9, 23.2] m/s, which is only slightly lower than the mean wind speed of [24.0, 27.9] m/s inferred from hail-induced TIL damage. Such a small difference between the estimates of mean wind speed indicates that, given a known correlation between the hail-induced TIL damage and the kinetic energy of hailstones, it is feasible to infer the wind speed based on the observations of hail-induced TIL damage.

4.3. Wind direction retrieval from hail-induced damage

Previous studies pointed out that the wind direction during an extreme event can also be inferred according to the fall directions of vegetation such as trees (Rhee and Lombardo, 2018), whereas such method may be inapplicable in a built environment where a large field of vegetation is uncommon. This study proposes an alternative approach to infer the wind direction based on the hail-induced TIL damage on building facades. It was observed through in-situ investigation that, in the vast majority of the TIL damage cases, only the TILs on the West (including Southwest and Northwest) facades were damaged by hailstone impacts. Therefore, to properly reflect the orientations of damaged facades, Fig. 19 shows the locations of TIL damage cases by arrows that point towards the buildings perpendicularly to the damaged facades. It is noteworthy that these arrows do not necessarily represent the exact horizontal direction of hailstone impacts, because the hailstones might have approached the facades obliquely instead of perpendicularly. As shown in Fig. 16, the hailstone impacted the TILs generally from the West, which agrees with the outflow direction over the city when heavy precipitation started at around 18:18 UTC. The reason behind the evident correlation between the orientations of damaged facades and the outflow direction is intuitively understandable, that is, the horizontal motions of hailstones that are responsible for the impacts to vertical surfaces are driven by wind force. Based on these observations, it is suggested that the hail-induced damage to building facades can be utilized as an indicator of the wind direction during a thunderstorm event.

5. Concluding remarks

Based on the in-situ meteorological data and the post-event damage survey, this paper analyzed the damage to low-rise buildings in Sânnicolau Mare caused by an intense thunderstorm on June 25th, 2021.

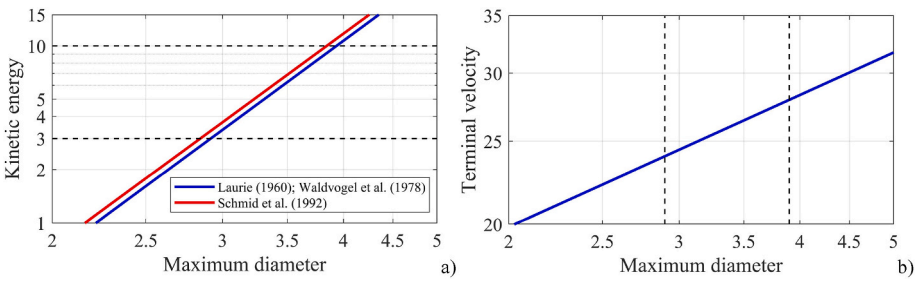

Fig. 18. Correlations of maximum diameter of a hailstone with (a) kinetic energy and (b) terminal velocity.

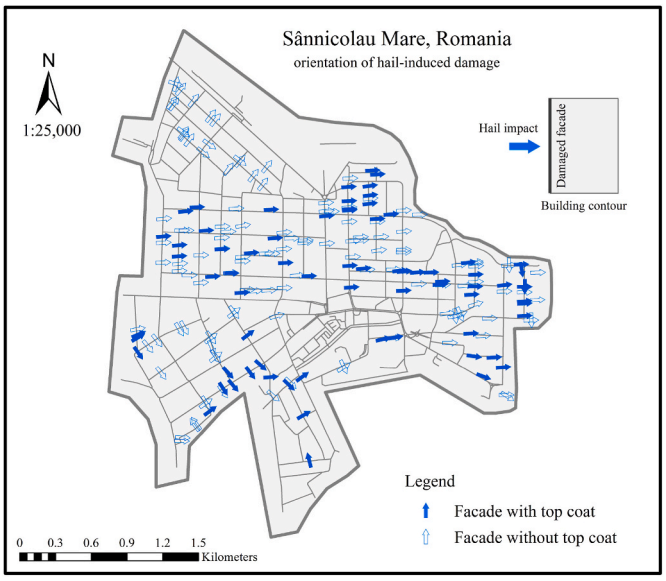

Fig. 19. Locations and orientations of hail-induced TIL damage cases.

Anemometric records showed that the maximum instantaneous wind speed reached 40.6 m/s during the thunderstorm, and the survey identified a total number of 237 building damage cases in the urban area. In this study, the mechanisms behind the wind- and hail-induced building damage were discussed, the economic loss caused by roof and TIL damage was evaluated, the estimation scales for wind intensities were validated, the approach to utilize the hail-induced damage to building facades as a new indicator for the estimation of wind speed and direction was proposed. The main findings of this study are presented as follows:

1. According to the post-event survey, the building roofing system failure was the most common wind-induced damage type. Noticeable damage was observed from the roofs made of sheet metal and clay tiles. It is inferred that the roof damage was mainly attributed to the excessive negative pressures caused by the flow separations near roof edges and ridges. This roof damage pattern during the thunderstorm is similar to that during tropical cyclones as reported in previous studies.
2. According to the mechanisms behind the wind-induced damage to a typical church (i.e., Building A), two practical wind-resistant measures for similar structures are highlighted herein. First, the connection between the roof and the lower structure, especially near the roof edges and corners, shall be adequately enhanced to endure the suction force induced by flow separation. Second, to avoid the internal pressure from increasing drastically and leading to a higher probability of roof failure, the openings such as windows and doors shall be sealed properly to prevent the wind flow from entering the building through them.
3. Based on the observations of wind-induced roof damage and the in-situ anemometric records of the thunderstorm, the F-scale, the EF-scale and its two adaptive versions (Canadian and Japanese EF-scales) were validated. The results indicated that, although originally proposed for the estimation of tornado wind speed, all these scales, especially the EF-scales, can also serve as a reliable tool to estimate the intensity of thunderstorms.
4. Driven by the high horizontal winds of the thunderstorm outflow, the hailstones caused significant damage to the facades of a large number of buildings, especially on the TILs without the top coat. A prominent correlation was found between the orientations of these damaged facades and the wind direction of thunderstorm outflow, suggesting that the hail-induced damage to building facades can be utilized to infer the wind direction. This finding is particularly important to the post-event analysis of extreme wind events over urban areas.
5. Based on the field observations of hail-induced TIL damage and the experimental results reported in literature, the horizontal mean wind speed during the hail precipitation was estimated. Such estimated wind speed reasonably agreed with the in-situ anemometric records, indicating that it is feasible to employ the hail-induced TIL damage as an indicator
6. Estimates of total economic loss for this particular event showed that the repair costs associated with hail-induced damage resulted much larger than those associated with wind-induced damage. Although the hail-induced damage to structures is widely recognized and may be financially compensated by insurance, these compensations are typically for severe damage cases such as penetrated rooftops by hail impact. For the surveyed buildings in this study, the hail-induced facade damage is only categorized as a cosmetic damage in Romania (i.e., not interfering with the function of the damaged area) and it is not covered by insurance companies, posing a significant financial burden for building owners.

The present research opens to many perspectives and future work. Post-event surveys after thunderstorm events will be analyzed systematically in order to enhance the knowledge of the mechanisms behind the wind-induced damage due to downburst and to improve the wind intensity scales and economic loss evaluations accordingly. In particular, regarding the hail damage that have yet been discussed in detail in literature, further studies will be carried out based on the survey data collected by this study. These future perspectives include but are not limited to: (1) The hail damage distribution on different facades, to be automatically identified from site photos by an image processing algorithm, may be analyzed to better understanding the mechanism and pattern of hail damage; (2) Hail pads may be deployed at multiple locations of the area before the thunderstorm events to collect more comprehensive information such as the hailstone size and the density of hail impact; (3) Experiments may be conducted in laboratories to better quantify the relationship between the hail damage on TILs and the wind speed.

CRediT authorship contribution statement

Ileana Calotescu: Conceptualization, Methodology, Formal analysis, Investigation, Resources, Writing – review & editing. **Xiao Li:** Conceptualization, Methodology, Formal analysis, Investigation, Writing – original draft. **Mekdes T. Mengistu:** Investigation, Writing – review & editing. **Maria Pia Repetto:** Conceptualization, Resources, Writing – review & editing, Supervision, Project administration, Funding acquisition.

Declaration of competing interest

The authors declare that they have no known competing financial interests or personal relationships that could have appeared to influence the work reported in this paper.

Data availability

The data that has been used is confidential.

Acknowledgement

The research carried out for this paper is funded by the European Research Council (ERC) under the European Union's Horizon 2020 research and innovation program (grant agreement No. 741273) for the Project THUNDERR - Detection, simulation, modelling and loading of thunderstorm outflows to design wind-safer and cost-efficient structures

– supported by an Advanced Grant (AdG) 2016. The authors are grateful to Meteo Romania for providing the hourly wind data used within this paper.

References

Aboutabikh, M., Ghazal, T., Chen, J., Elgamal, S., Aboshosha, H., 2019. Designing a blade-system to generate downburst outflows at boundary layer wind tunnel. J. Wind Eng. Ind. Aerod. 186, 169–191. https://doi.org/10.1016/j.jweia.2019.01.005.

Beekmans, C., Schween, J., Lennefer, M., Simmer, C., 2021. Comparison of cloud motion vector profiles derived from ground-based hemispheric stereocameras to wind-lidar observations. Meteorol. Z. 30, 503–513. https://doi.org/10.1127/metz/2021/1069.

Blong, R., 2004. Residential building damage and natural perils: Australian examples and issues. Build. Res. Inf. 32, 379–390. https://doi.org/10.1080/0961321042000221007.

Brusco, S., Buresti, G., Lo, Y.-L., Piccardo, G., 2022. Constant-frequency time cells in the vortex-shedding from a square cylinder in accelerating flows. J. Wind Eng. Ind. Aerod. 230, 105182 https://doi.org/10.1016/j.jweia.2022.105182.

Burcea, S., Cică, R., Bojariu, R., 2016. Hail climatology and trends in Romania: 1961–2014. Mon. Weather Rev. 144, 4289–4299. https://doi.org/10.1175/MWR-D-16-0126.1.

Burlando, M., Zhang, S., Solari, G., 2018. Monitoring, cataloguing, and weather scenarios of thunderstorm outflows in the northern Mediterranean. Nat. Hazards Earth Syst. Sci. 18, 2309–2330. https://doi.org/10.5194/nhess-18-2309-2018.

Byers, H.R., Braham, R.R., 1949. The Thunderstorm: Final Report of the Thunderstorm Project. U.S. Government Printing Office, Washington, DC.

Calotescu, I., 2019. Damage from recent thunderstorms in Romania. Lecture Notes in Civil Engineering. https://doi.org/10.1007/978-3-030-12815-9_12.

Calotescu, I., Chitez, A.S., Bîrsan, M.V., 2022. A thunderstorm hazard map based on recent wind events in Romania. In: Proceedings of the International Conference on Natural Hazards and Infrastructure. ICONHIC2022, Athens.

Calotescu, I., Repetto, M.P., 2022. Monitoring of thunderstorm activity in Sânnicolau Mare, Romania. In: Calotescu, I., Chitez, A.S., Coșoiu, C., Vlăduț, C.A. (Eds.), 8th European-African Conference on Wind Engineering (8EACWE2022). Conspress București, Bucharest, pp. 479–482. https://doi.org/10.5281/zenodo.8092030.

Canepa, F., Burlando, M., Romanic, D., Solari, G., Hangan, H., 2022. Experimental investigation of the near-surface flow dynamics in downburst-like impinging jets. Environ. Fluid Mech. 22, 921–954. https://doi.org/10.1007/s10652-022-09870-5.

Canepa, F., Burlando, M., Solari, G., 2020. Vertical profile characteristics of thunderstorm outflows. J. Wind Eng. Ind. Aerod. 206, 104332 https://doi.org/10.1016/j.jweia.2020.104332.

Chen, L., Letchford, C.W., 2004. Parametric study on the along-wind response of the CAARC building to downbursts in the time domain. J. Wind Eng. Ind. Aerod. 92, 703–724. https://doi.org/10.1016/j.jweia.2004.03.001.

Chitez, A.S., Calotescu, I., Bîrsan, M.V., 2022. An updated map of damaging winds in Romania. In: Calotescu, I., Chitez, A., Coșoiu, C., V, A. (Eds.), 8th European-African Conference on Wind Engineering (8EACWE2022). Conspreess București, pp. 323–326.

Chmielewski, T., Nowak, H., Walkowiak, K., 2013. Tornado in Poland of august 15, 2008: results of post-disaster investigation. J. Wind Eng. Ind. Aerod. 118, 54–60. https://doi.org/10.1016/j.jweia.2013.04.007.

Choi, E.C.C., Hidayat, F.A., 2002. Dynamic response of structures to thunderstorm winds. Prog. Struct. Eng. Mater. 4, 408–416. https://doi.org/10.1002/pse.132.

Cox, D., Arikawa, T., Barbosa, A., Guannel, G., Inazu, D., Kennedy, A., Li, Y., Mori, N., Perry, K., Prevatt, D., Roueche, D., Shimozono, T., Simpson, C., Shimakawa, E., Shimura, T., Slocum, R., 2019. Hurricanes irma and Maria post-event survey in US Virgin Islands. Coast Eng. J. 61, 121–134. https://doi.org/10.1080/21664250.2018.1558920.

CR1-1-4, 2012. Normativ privind calculul construcțiilor și elementelor de construcții. CR 1-1-4/2012 Cod de proiectare. Evaluarea acțiunii vântului aspra construcțiilor. Matrix Rom. 22–23.

Davenport, A., 1961. The application of statistical concepts to the wind loading of structures. Proc. Inst. Civ. Eng. 19 https://doi.org/10.1680/iicep.1961.11304.

De Gaetano, P., Repetto, M.P., Repetto, T., Solari, G., 2014. Separation and classification of extreme wind events from anemometric records. J. Wind Eng. Ind. Aerod. 126, 132–143. https://doi.org/10.1016/j.jweia.2014.01.006.

Durst, C.S., 1960. Wind speeds over short periods of time. Meteorol. Mag. 89, 181–187.

EN1991-1-4, 2005. Eurocode 1: Actions on Structures - Part 1-4. General Actions - Wind Actions.

Environment Canada, 2022. Enhanced Fujita Scale for Wind Damage. Canada.

Feuerstein, B., Groenemeijer, P., Dirksen, E., Hubrig, M., Holzer, A.M., Dotzek, N., 2011. Towards an improved wind speed scale and damage description adapted for Central Europe. Atmos. Res. 100, 547–564. https://doi.org/10.1016/j.atmosres.2010.12.026.

Francke, B., Zamorowska, R., 2020. Resistance of External Thermal Insulation Composite Systems with Rendering (ETICS) to Hail. Materials. https://doi.org/10.3390/ma13112452.

Fujita, T.T., 1985. THE DOWNBURST MICROBURST and MACROBURST Report of Projects NIMROD and JAWS.

Fujita, T.T., 1978. Manual of Downburst Identification for Project NIMROD. Satellite and Mesemeteorology Research Paper 156. Dept. of Geophysical Sciences, University of Chicago, 104pp. [NTIS PB-286048].

Fujita, T.T., 1971. Proposed Characterization of Tornadoes and Hurricanes by Area and Intensity. SMRP Research Paper Nr, p. 91.

Fujita, T.T., Smith, B.E., 1993. Aerial survey and photography of tornado and microburst damage. In: The Tornado: its Structure, Dynamics, Prediction, and Hazards. Geophysical Monograph Series, pp. 479–493. https://doi.org/10.1029/GM079p0479.

Ghazal, T., Aboutabikh, M., Aboshosha, H., Abdelwahab, M., 2022. Thunderstorm wind load evaluation on storm shelters using wind tunnel testing. Eng. Struct. 262, 114350 https://doi.org/10.1016/j.engstruct.2022.114350.

Hao, H., Wang, Y., 2020. Leveraging multimodal social media data for rapid disaster damage assessment. Int. J. Disaster Risk Reduc. 51, 101760 https://doi.org/10.1016/j.ijdrr.2020.101760.

Heymsfield, A., Szakáll, M., Jost, A., Giammanco, I., Wright, R., 2018. A comprehensive observational study of graupel and hail terminal velocity, mass flux and kinetic energy. J. Atmos. Sci. 75 https://doi.org/10.1175/JAS-D-18-0035.1.

Hjelmfelt, M.R., 1988. Structure and life cycle of microburst outflows observed in Colorado. J. Appl. Meteorol. Climatol. 27, 900–927. https://doi.org/10.1175/1520-0450(1988)027<0900:SALCOM>2.0.CO;2.

Japan Meteorological Agency, 2015. Guideline for the Japanese Enhanced Fujita Scale.

Jubayer, C., Elatar, A., Hangan, H., 2016. Pressure distributions on a low-rise building in a laboratory simulated downburst. In: 8th International Colloquium on Bluff Body Aerodynamics and Applications Northeastern University. Boston, Massachusetts, USA June 7 - 11, 2016.

Koks, E.E., Haer, T., 2020. A high-resolution wind damage model for Europe. Sci. Rep. 10, 6866. https://doi.org/10.1038/s41598-020-63580-w.

Kopp, G.A., Morrison, M.J., Henderson, D.J., 2012. Full-scale testing of low-rise, residential buildings with realistic wind loads. J. Wind Eng. Ind. Aerod. 104 (106), 25–39. https://doi.org/10.1016/j.jweia.2012.01.004.

Kunz, M., Sander, J., Kottmeier, Ch, 2009. Recent trends of thunderstorm and hailstorm frequency and their relation to atmospheric characteristics in southwest Germany. Int. J. Climatol. 29, 2283–2297. https://doi.org/10.1002/joc.1865.

Laurie, J.A.P., 1960. Hail and its Effects on Buildings. Council for Scientific and Industrial Research, Pretoria, South Africa.

Le, V., Caracoglia, L., 2020. Experimental investigation on non-stationary wind loading effects generated with a multi-blade flow device. J Fluids Struct 96, 103049. https://doi.org/10.1016/j.jfluidstructs.2020.103049.

Leatherman, S.P., Chowdhury, A.G., Robertson, C.J., 2007. Wall of wind full-scale destructive testing of coastal houses and hurricane damage mitigation. J. Coast Res. 23, 1211–1217.

Letchford, C.W., Mans, C., Chay, M.T., 2002. Thunderstorms - their importance in wind engineering (a case for the next generation wind tunnel). J. Wind Eng. Ind. Aerod. 90, 1415–1433. https://doi.org/10.1016/S0167-6105(02)00262-3.

Lombardo, F.T., Mason, M.S., de Alba, A.Z., 2018. Investigation of a downburst loading event on a full-scale low-rise building. J. Wind Eng. Ind. Aerod. 182, 272–285. https://doi.org/10.1016/j.jweia.2018.09.020.

Lombardo, F.T., Smith, D.A., Schroeder, J.L., Mehta, K.C., 2014. Thunderstorm characteristics of importance to wind engineering. J. Wind Eng. Ind. Aerod. 125, 121–132. https://doi.org/10.1016/j.jweia.2013.12.004.

Loredo-Souza, A.M., Lima, E.G., Vallis, M.B., Rocha, M.M., Wittwer, A.R., Oliveira, M.G. K., 2019. Downburst related damages in Brazilian buildings: are they avoidable? J. Wind Eng. Ind. Aerod. 185, 33–40. https://doi.org/10.1016/j.jweia.2018.11.022.

Mason, M.S., Lo, Y., 2019. Wind loading of the CAARC building during velocity profile transitions, Part 1: transient pressure coefficient distributions. In: Proceedings of the 15th International Conference on Wind Engineering, pp. 829–830.

McDonald, J.R., Metha, K.C., 2004. A Recommendation for an Enhanced Fujita Scale (EF-Scale). Wind Science and Engineering Center. Texas Tech University.

MDLPA, 2010. Hotarâre privind aprobarea standardelor de cost pentru obiective de investiții finanțate din fonduri publice. Monitorul Oficial al României, Partea I. Nr. 311/12.V.2010.

Mengistu, M.T., Orlando, A., Repetto, M.P., 2023. Wind and structural response monitoring of a lighting pole for the study of downburst effects on structures. J. Wind Eng. Ind. Aerod. 240, 1016/j.jweia.2023.105447.

Meloy, N., Sen, R., Pai, N., Mullins, A., 2007. Roof damage in new homes caused by hurricane charley. Journal of Performance of Constructed Facilities - J PERFORM CONSTR FACIL 21. https://doi.org/10.1061/(ASCE)0887-3828(2007)21:2(97).

Palencia, C., Berthet, C., Massot, M., Castro, A., Dessens, J., Fraile, R., 2007. On the individual calibration of hailpads. Atmos. Res. 83, 493–504. https://doi.org/10.1016/j.atmosres.2006.04.002.

Paterson, D.A., Sankaran, R., 1994. Hail impact on building envelopes. J. Wind Eng. Ind. Aerod. 53, 229–246. https://doi.org/10.1016/0167-6105(94)90028-0.

Pistotnik, G., Holzer, A.M., Kaltenböck, R., Tschannett, S., 2011. An F3 downburst in Austria—a case study with special focus on the importance of real-time site surveys. Atmos. Res. 100, 565–579. https://doi.org/10.1016/j.atmosres.2010.10.011.

Pita, G.L., de Schwarzkopf, M.L.A., 2016. Urban downburst vulnerability and damage assessment from a case study in Argentina. Nat. Hazards 83, 445–463. https://doi.org/10.1007/s11069-016-2323-z.

Potter, S., 2007. Fine-Tuning Fujita: after 35 years, a new scale for rating tornadoes takes effect. Weatherwise 60, 64–71.

Powell, M.D., Houston, S.H., 1996. Hurricane andrew's landfall in South Florida. Part II: surface wind fields and potential real-time applications. Weather Forecast. 11, 329–349. https://doi.org/10.1175/1520-0434(1996)011<0329:HALISF>2.0.CO;2.

Punge, H.J., Kunz, M., 2016. Hail observations and hailstorm characteristics in Europe: a review. Atmos. Res. 176–177, 159–184. https://doi.org/10.1016/j.atmosres.2016.02.012.

Rädler, A.T., Groenemeijer, P.H., Faust, E., Sausen, R., Púčik, T., 2019. Frequency of severe thunderstorms across Europe expected to increase in the 21st century due to

rising instability. NPJ Clim Atmos Sci 2, 30. https://doi.org/10.1038/s41612-019-0083-7.
Rhee, D.M., Lombardo, F.T., 2018. Improved near-surface wind speed characterization using damage patterns. J. Wind Eng. Ind. Aerod. 180, 288–297.
Romanian National Institute of Statistics [WWW Document], 2011. URL. https://www.recensamantromania.ro/rpl-2011/rezultate-2011/.
Schmid, W., Schiesser, H., Waldvogel, A., 1992. The kinetic energy of hailfalls. Part IV: patterns of hailpad and radar data. Journal of Applied Meteorology - J APPL METEOROL 31, 1165–1178. https://doi.org/10.1175/1520-0450(1992)031<1165:TKEOHP>2.0.CO;2.
Solari, G., 2014. Emerging issues and new frameworks for wind loading on structures in mixed climates. Wind and Structures. Int. J. 19, 295–320. https://doi.org/10.12989/was.2014.19.3.295.
Solari, G., 1993. Gust buffeting. I: peak wind velocity and equivalent pressure. J. Struct. Eng. 119, 365–382. https://doi.org/10.1061/(ASCE)0733-9445(1993)119:2(365).
Solari, G., Burlando, M., De Gaetano, P., Repetto, M.P., 2015. Characteristics of thunderstorms relevant to the wind loading of structures. Wind and Structures. Int. J. 20, 763–791. https://doi.org/10.12989/was.2015.20.6.763.
Solari, G., Burlando, M., Repetto, M.P., 2020. Detection, simulation, modelling and loading of thunderstorm outflows to design wind-safer and cost-efficient structures. J. Wind Eng. Ind. Aerod. 200, 104142 https://doi.org/10.1016/j.jweia.2020.104142.
Stott, P.A., Christidis, N., Otto, F.E.L., Sun, Y., Vanderlinden, J.-P., van Oldenborgh, G.J., Vautard, R., von Storch, H., Walton, P., Yiou, P., Zwiers, F.W., 2016. Attribution of extreme weather and climate-related events. WIREs Climate Change 7, 23–41. https://doi.org/10.1002/wcc.380.
Tamura, Y., 2009. Wind-induced damage to buildings and disaster risk reduction. In: The Seventh Asia-Pacific Conference on Wind Engineering. Novem-Ber, Taipei, Taiwan, pp. 8–12.
Waldvogel, A., Schmid, W., Federer, B., 1978. The kinetic energy of hailfalls. Part I: hailstone spectra. Journal of Applied Meteorology - J APPL METEOROL 17, 515–520. https://doi.org/10.1175/1520-0450(1978)017<0515:TKEOHP>2.0.CO;2.
Wood, G.S., Kwok, K.C.S., Motteram, N.A., Fletcher, D.F., 2001. Physical and numerical modelling of thunderstorm downbursts. J. Wind Eng. Ind. Aerod. 89, 535–552. https://doi.org/10.1016/S0167-6105(00)00090-8.
Xhelaj, A., Burlando, M., Solari, G., 2020. A general-purpose analytical model for reconstructing the thunderstorm outflows of travelling downbursts immersed in ABL flows. J. Wind Eng. Ind. Aerod. 207, 104373 https://doi.org/10.1016/j.jweia.2020.104373.
Yuan, F., Liu, R., 2018a. Feasibility study of using crowdsourcing to identify critical affected areas for rapid damage assessment: hurricane Matthew case study. Int. J. Disaster Risk Reduc. 28, 758–767. https://doi.org/10.1016/j.ijdrr.2018.02.003.
Yuan, F., Liu, R., 2018b. Crowdsourcing for forensic disaster investigations: hurricane Harvey case study. Nat. Hazards 93, 1529–1546. https://doi.org/10.1007/s11069-018-3366-0.
Zhang, S., Solari, G., De Gaetano, P., Burlando, M., Repetto, M.P., 2018. A refined analysis of thunderstorm outflow characteristics relevant to the wind loading of structures. Probabilist. Eng. Mech. 54, 9–24. https://doi.org/10.1016/j.probengmech.2017.06.003.